Journal of Photochemistry and Photobiology A: Chemistry 216 (2010) 228–237

Contents lists available at ScienceDirect

Journal of Photochemistry and Photobiology A: Chemistry

journal homepage: www.elsevier.com/locate/jphotochem

Photocatalytic initiation of electroless deposition

Michael A. Bromley[a], Colin Boxall[a,*], Sarah Galea[b], Philip S. Goodall[c], Simon Woodbury[c]

[a] Engineering Department, Lancaster University, Lancaster LA1 4YR, UK
[b] Centre for Materials Science, University of Central Lancashire, Preston PR1 2HE, UK
[c] Central Laboratory, National Nuclear Laboratory, Sellafield, Seascale, Cumbria CA20 1PG, UK

ARTICLE INFO

Article history:
Available online 30 July 2010

Keywords:
Photocatalysis
Electroless deposition
Titanium dioxide
Quartz crystal microbalance

ABSTRACT

We report a one-step photocatalytically initiated electroless deposition (PIED) process that allows for the photogeneration of robust, coherent, conducting metal layers on semiconductor-sensitised insulator surfaces. The PIED process involves two steps, performed simultaneously in the same metal precursor solution:

(i) Metal nanoparticles are formed at the surface of the semiconductor by photocatalytic reduction of an appropriate metal precursor.
(ii) The nanoparticles then serve as nucleation centres for an autocatalytic electroless deposition process, growing and coalescing to form a continuous metal layer.

Layers of various metals including Ag and Pd have been generated by PIED on mesoporous TiO_2 (m-TiO_2) coated quartz glass slides and PVDF membranes. Deposition occurs only onto areas of the substrate both sensitised with TiO_2 and irradiated with ultra-band gap energy light. The morphology of the resultant layer is dependent upon the nucleation density occurring during the primary photocatalytic stage of PIED. PIED provides a cheaper, environmentally cleaner and more controllable option than traditional techniques of plating onto dielectric surfaces.

1. Introduction

Electroless deposition is a plating process in which metal ions are deposited from solution onto a substrate through their reduction by a chemical reducing agent [1]. As the process is independent of electrical current it can be used to deposit metals onto an insulating surface, something which is not possible through electroplating techniques. The reaction is dependent on catalysis of metal ion reduction by the substrate surface whilst deposition elsewhere is minimised. The deposited metal must also catalyse the reduction if further deposition is to occur when the substrate surface is completely covered [2]. Electroless plating is most commonly performed with Cu, Ni, Co and precious metals with plating solutions being usually comprised of the metal salt, a reducing agent, a buffer and complexing agents to stabilise.

The use of electroless plating on insulating surfaces usually involves sensitisation of the substrate in order for it to catalyse the deposition process, Fig. 1(a) and (b) [2,3]. Typically a catalytic metal such as palladium would be seeded onto the substrate, most usually in a two-step process, Fig. 1(a); first, pre-sensitisation of the substrate with a tin chloride solution in hydrochloric acid resulting in the adsorption of Sn^{2+} ions to the surface; second, treatment with a palladium chloride solution in hydrochloric acid during which Sn^{2+} ions on the surface reduce solution Pd(II) ions to form nucleation deposits on the substrate surface [2]. A recent improvement, Fig. 1(b), combines sensitising and nucleating ions in a single solution. This results in adsorption of Sn–Pd particles with the Sn then removed with concentrated HCl to expose the Pd catalyst [4]. Each method has disadvantages; the sensitisation processes must be repeated several times to achieve a sufficiently catalytic surface, which can be costly and time consuming; lengthy surface preparation involving cleaning, etching and neutralising is required to promote bond formation; and the resulting metal deposit will contain Pd and Sn, the latter being a particularly troublesome impurity for electrochemically based applications.

As an alternative to electrochemical activation, metallic nuclei may be generated photochemically. We report on a one-step photocatalytic method, photocatalytically initiated electroless deposition (PIED), by which metal nucleation centres may be photochemically generated directly onto semiconductor particles/surfaces. This method, presented in outline in Figs. 1(c) and 2,

* Corresponding author. Tel.: +44 1524 593109; fax: +44 1524 592777.
E-mail addresses: m.bromley@lancaster.ac.uk (M.A. Bromley), c.boxall@lancaster.ac.uk (C. Boxall), philip.s.goodall@nnl.co.uk (P.S. Goodall), simon.woodbury@nnl.co.uk (S. Woodbury).

1010-6030/$ – see front matter © 2010 Elsevier B.V. All rights reserved.
doi:10.1016/j.jphotochem.2010.07.029

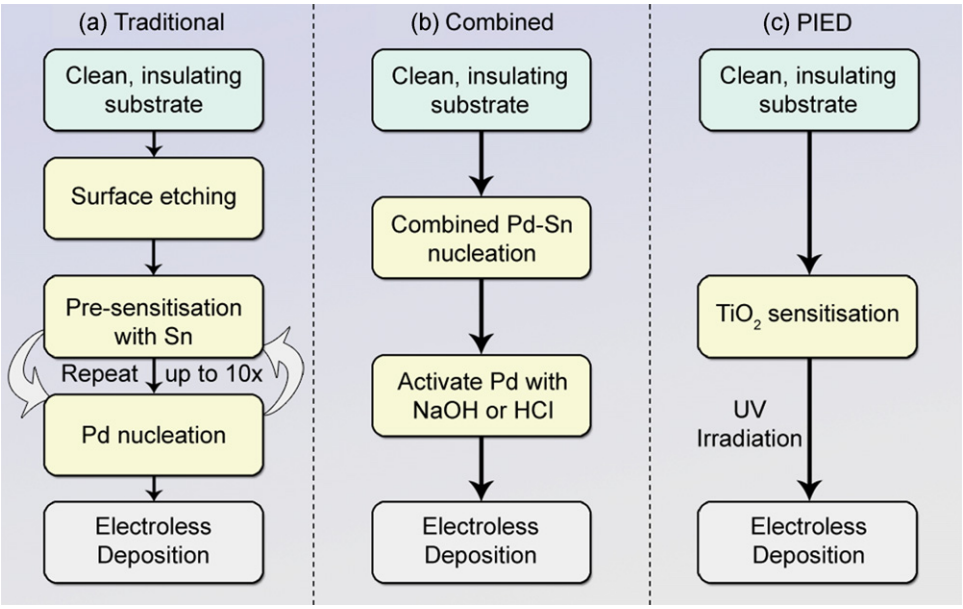

Fig. 1. Flow diagrams for electroless deposition routes involving: (a) sequential Sn–Pd sensitisation; (b) combined Sn–Pd sensitisation; (c) photocatalytic initiation (PIED).

utilises the photocatalytic properties of TiO_2 to initiate electroless deposition for surface metallisation.

Semiconductor particles, such as TiO_2, SnO_2, WO_3, can act as efficient photocatalysts for a range or processes such as pollution abatement [5], corrosion inhibition [6], precious metal recovery [7,8] and heavy element removal from effluent streams [9]. In these reactions, absorption of ultra-band gap energy photons generate electron–hole pairs within the semiconductor particles, Fig. 2(i). These charge carriers can react with species in solution, effecting oxidation and reduction reactions and performing useful electrochemistry. Such reactions may include the electrodeposition of metal ions to form metal nucleates at the semiconductor surface through the action of the photogenerated electrons.

Metallisation of semiconductors by photocatalytic reduction of metal precursors is an established technology [9], primarily developed to improve the efficiency of TiO_2 for O_2 reduction [8] or H_2O oxidation [10]. For example, Stathatos et al. [11] described the photocatalytic deposition of Ag nanoparticles onto m-TiO_2 films through a single electron transfer photoreduction. However, the result of such a process is typically is a nanoparticle coating rather than a coherent metallic layer.

The photocatalytic generation of such metal nanoparticles at semiconductor surfaces offers an alternative to the electrochemical metal nucleation methods employed in conventional electroless deposition shown in Fig. 1(a) and (b). Once metal nucleation sites have been formed by photocatalytic means then, in the presence of an appropriate reductant, further deposition can occur onto those nucleate sites by conventional electroless deposition reactions, Fig. 2(ii). These are the principal steps of PIED. As such, PIED may obviate the need for Sn–Pd catalysts so eliminating contamination from prior nucleation whilst the fewer steps and materials required may provide a cheaper, environmentally cleaner and (through control of incident light intensity) more controllable option than the usually employed methods for dielectric plating.

Two generic embodiments of PIED may be envisaged. In the first embodiment, the reductant or hole scavenger employed during the photocatalytic initiation step (Fig. 2(i)) is a different reagent to the reductant employed during the autocatalytic electroless deposition/metal nucleate growth step (Fig. 2(ii)). In this context, the photoinitiated nuclei formation and growth steps can be performed in two ways: first, by immersion of the surface to be coated in a hole scavenger/precursor metal ion solution followed by a second immersion in a reductant/metal ion solution, so-called "two-step" PIED; and second, by immersion of the substrate in a solution containing the precursor metal ion and both the hole scavenger and reductant, so-called "one-step" PIED. In the second generic embodiment, the hole scavenger and the reductant for the metal growth step are the same and so this may be classified as a "one-step" PIED process. It is this latter embodiment that is the subject of this communication.

Coupled photocatalytic and electroless deposition of Pd using TiO_2 as a catalyst has been reported previously by Wu et al. [12,13]. Pd deposition was achieved in a two-step process using methanol as a hole scavenger and hydrazine as a reductant. The same team have

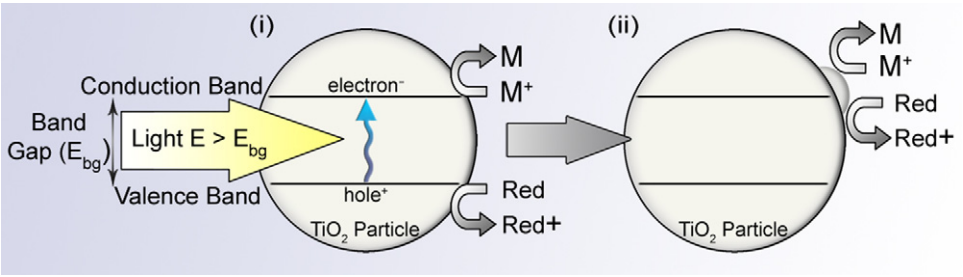

Fig. 2. Two stages of PIED: (i) the photocatalytic process derived from interfacial electron transfer at a photoexcited semiconductor particle and (ii) the autocatalytic electroless deposition process.

also reported the deposition of Pd onto alumina discs by a similar method [14,15]. Yang et al. [16] report a one-step process for photoinitiated deposition of Cu onto ZnO sensitised substrates under UV irradiation. However, ZnO readily photocorrodes [17] suggesting this process could be driven by galvanic displacement rather than metal ion reduction by photogenerated electrons. A galvanic displacement mechanism would lead to the incorporation of metallic Zn into the electrolessly deposited metal, an undesirable effect for reasons of deposit purity (vide supra).

In light of the above, we describe generation of Ag and Pd layers on TiO_2-sensitised insulator substrates in true one-step PIED for the first time. Use of TiO_2 obviates semiconductor photocorrosion whilst deposition of Ag and Pd allows for study of 1 and 2 electron reduction PIED processes. Of relevance to process development is that well studied, conventional electroless deposition recipes are available for both metals wherein the reductants have also been used as hole scavengers in TiO_2 photocatalysis. These reductants are of differing reducing power, allowing inferences to be made regarding the effect of this parameter on deposit morphology.

2. Experimental

2.1. Materials and reagents

All reagents used are AnalaR grade or higher, and purchased from Sigma–Aldrich (Gillingham, Dorset, UK) or Alfa Aesar (Heysham, Lancashire, UK). Doubly distilled water, further purified by a deionisation system (E-pure model 04642, Barnstead/Thermodyne, Dubuque, IA, USA) to a resistivity of $1.8 \times 10^5\ \Omega$ m. Nitrogen Whitespot grade is provided by BOC Ltd., Guildford, Surrey, UK.

2.2. TiO_2 sensitisation of substrates using a reverse micelle sol–gels

Quartz substrates were coated with a mesoporous TiO_2 (m-TiO_2) layer via sol–gel spin coating. A reverse micellar sol–gel, as described by Yu et al. [18], was prepared by vigorously mixing Triton X-100 (26.0 g) and cyclohexane (150 ml) to form a reverse micellar solution. After 30 min water (1.08 g) is added and the solution appears turbid. This clears upon addition of titanium (IV) isopropoxide (99.999%, 23 g). The solution was then stirred for 60 min at 293 K, so forming a colloid of TiO_2 nanoparticles. Acetylacetone (10 ml) is added to stabilise the solution. The resultant sol–gel is applied to substrates by spin coating for 5 s at 2900 rpm using an inverted model 636 rotating disk electrode system (Princeton Applied Research, Tennessee, USA). Coated substrates are then fired in a furnace at 500 °C for 1 h to anneal the TiO_2 and produce a resilient coating. Annealing at this temperature produces TiO_2 with predominantly anatase structure and coatings are composed of interconnected, mono-dispersed, spherical primary particles approximately 10 nm in diameter within a mesoporous structure (vide infra). Phase identification was achieved through Raman spectroscopy using a Renishaw Ramascope 1000 (Renishaw, Gloucestershire, UK) with back-scattering geometry and a 17 mW He–Ne (632.8 nm) laser. UV–vis spectra of films were obtained using UV–vis spectrophotometry (Hewlett-Packard 8452A, Bristol, United Kingdom). Surface topography, roughness, etc., were assessed using atomic force microscopy (AFM; Q-Scope 250, Quesant, CA, USA). Sensitised substrates were stored in darkness at room temperature prior to use.

2.3. TiO_2 sensitisation of substrates using nanoparticulate sols

Polyvinylidene fluoride (PVDF) membranes (0.2 μm pore size, Millipore) are unable to withstand 500 °C annealing and so were sensitised by coating with a nanoparticulate TiO_2 sol (TiPE® O502, TitanPE Technologies Inc., Shanghai, China) deposited via spin coating (see above) for single side sensitisation and by manual dip-coating for two sided sensitisation. The sol contains nanoparticulate anatase TiO_2 with average primary particle size of <8 nm in water based solution. Coated PVDF membranes were oven dried at 100 °C to remove solvent and so produce a coating of anatase nanoparticles. Membranes were stored in darkness at room temperature prior to use.

2.4. Preparation of Ag electroless plating solution

Electroless Ag plating solutions were prepared to the composition given in Table 1. All components are added to a small quantity of distilled water in the order listed, ensuring full dissolution with each addition. The completed solution was made up to volume with distilled water and purged with N_2 for 20 min to deoxygenate. The pH of the solution was 11.5 and PIED was carried out at 298 K. Electroless plating solutions are freshly made immediately before use for optimum performance. As silver nitrate is light sensitive Ag solutions are prepared and stored in amber flasks in darkness.

2.5. Preparation of Pd electroless plating solution

Electroless Pd solutions, developed in these laboratories, were prepared to the composition given in Table 2. Palladium chloride, di-sodium EDTA and ammonium hydroxide (28%, w/v, NH_3 in water) were added and, to ensure formation of the Pd-amine complex, stirred with gentle heating until the solution cleared. The solution was cooled and hydrazine reducing agent added. The solution was then made up to volume with distilled water and purged with N_2 for 20 min. As above, electroless plating solutions were made immediately before use for optimum performance.

2.6. One-step photocatalytically initiated electroless deposition

TiO_2-sensitised substrates were placed directly into freshly prepared electroless plating solutions in a quartz reaction vessel for improved UV transmittance. A N_2 stream was bubbled through the plating solutions during deposition in order to purge the solution of oxygen which can compete with metal ions for reduction at the photocatalytic surface. The N_2 stream also provides a source of agitation to prevent local depletion of metal ions at the substrate surface. The reaction vessel was then placed inside a circular photoreactor (Lidam Scientific, Dartford, UK) comprised of two hemi-cylinders, each containing 6×8 W UVA lamps. A thermostated water supply may be passed through the incorporated jacket of the quartz vessel allowing for control of the plating solution temperature. Water flow is maintained by peristaltic pump and temperature controlled by a thermostatic water bath. Post-deposition the substrate is removed from the plating solution, rinsed with distilled water and dried in air. Microstructure of the resultant layers was imaged using SEM (FEI Quanta 200).

2.7. Measurement of kinetics of PIED onto TiO_2

Rates of metal deposition were measured *in situ* using a quartz crystal microbalance (QCM, Type 5510, Institute of Physical Chemistry, Warsaw, Poland) with an Autolab PGSTAT10 system (Windsor Scientific Ltd., Slough, UK), driven by GPES 4.5 software (Eco-Chemie, Utrecht, The Netherlands) allowing simultaneous QCM and chronopotentiometric measurements to be taken – electrochemical QCM (EQCM). The mass sensitive oscillators (PAN, Warsaw, Poland) were 14 mm diameter, AT cut, 10 MHz resonant frequency quartz crystals. 6 mm diameter Au films were vacuum deposited onto each side of the piezoelectric crystals as electrical contacts

Table 1
Composition of Ag electroless plating solution.

Role	Component	Concentration
Metal precursor	Silver nitrate	1.496 g dm^{-3} (equivalent to 8.8 mmol dm^{-3})
Complexant	Ethylenediamine	3.245 g dm^{-3}
Stabiliser	3,5-Diiodotyrosine	0.0017 g dm^{-3}
Reducing agent/scavenger	Potassium sodium tartrate	0.7356 g dm^{-3}
pH		11–12

Table 2
Composition of Pd electroless plating solution.

Role	Component	Concentration
Metal precursor	Palladium chloride	3.60 g dm^{-3} (equivalent to 20.3 mmol dm^{-3})
Complexant	Di-sodium EDTA	62.4 g dm^{-3}
Stabiliser	Ammonium hydroxide	350.0 cm^3 dm^{-3} (of 28%, w/v, ammonia solution)
Reducing agent/scavenger	Hydrazine	11.0 cm^3 dm^{-3} (of pure liquid hydrazine)
pH		11–12

and solution interfaces. The frequency was measured with a programmable frequency timer/counter (Philips PM6680 JFluke Mfg. Co., Inc., Everett, WA). Mass change (Δm) was calculated from the frequency change (Δf) by the Sauerbrey equation [19]:

$$\Delta m = -k \times \Delta f \quad (1)$$

where in this simplified form of Sauerbrey, k is the mass sensitivity of the 10 MHz crystal. The value of k was determined experimentally by combined microgravimetry and cyclic voltammetry during electrochemical deposition and dissolution of Ag [20]. This was found to be 1.242 ng Hz^{-1}, comparable to the theoretical value of 1.249 ng Hz^{-1} obtained using the full form of Sauerbrey equation [19].

Quantification metal deposition rate is useful for mechanistic analysis. This can be expressed as the rate of change of resonant frequency shift $d\Delta f/dt$ (units: Hz s^{-1}) or as the rate of change in the deposited layer thickness $d\tau/dt$ (units: nm min^{-1}). If it is assumed that the metal is depositing over the m-TiO_2 layer as a coherent deposit with the density of the bulk metal, these two rates are related as follows:

$$\frac{d\tau}{dt}(\text{nm min}^{-1}) = \frac{0.6k}{A\rho}\frac{d\Delta f}{dt}(\text{Hz s}^{-1}) \quad (2)$$

where k is in ng Hz^{-1}, A is the piezoelectrically active crystal area in cm^2 and ρ is the bulk density of the deposited metal in g cm^{-3} (10.5 g cm^{-3} for Ag, 11.4 g cm^{-3} for Pd).

Chronopotentiometry was conducted using a saturated calomel electrode (SCE) as a reference (EIL, Chertsey, Surrey, UK) and Pt wire of 2.5×10^{-4} m Ø, 99.99+% purity (Advent Research Materials Ltd., Halesworth, Suffolk, UK) as a counter electrode.

Quartz crystals were coated with m-TiO_2 via the reverse micellar sol–gel spin-coating method of Section 2.2. A bespoke stage was fitted to the rotating disk electrode system to hold the crystal. The stage allowed coating of the Au crystal face whilst masking the contacts at the outer edge. Coated crystals were annealed at 350 °C for 1 h.

EQCM experiments were performed in a ground floor laboratory sited directly on building foundations and isolated from heavy machinery and vibration sources. For experiments conducted under illumination, monochromated 315 nm light from a 900 W Xe lamp was used to irradiate the crystal face through a quartz beaker. Both Δf and chronopotentiometric measurements were made during (photocatalytically initiated) electroless deposition onto (i) bare, Au-coated quartz piezoelectrodes, (ii) m-TiO_2-coated piezoelectrodes in the dark and (iii) m-TiO_2-coated piezoelectrodes irradiated with 315 nm light. The experimental set-up is in shown in Fig. 3.

3. Results and discussion

3.1. Characterization of m-TiO_2 layers on quartz glass substrates

Raman spectroscopy (supporting information (SI) 1) and XRD measurements (not shown) show that the films formed on quartz glass substrates and Au piezoelectrodes are predominantly anatase. UV–vis spectra (SI 2) indicate a band gap of 3.54 eV, blue shifted from the bulk value of 3.2 eV as the films are comprised of particles small enough to exhibit the quantum size effect. Atomic force microscopy (SI 3), indicated a constituent particle diameter of ~10 nm and maximum topographical height of 6 nm. Yu et al. [18] attribute a maximum thickness of 170 nm to the spin-coated layers.

3.2. One-step PIED of Ag and Pd on quartz glass and PVDF

Using the method of Section 2.6 and the solution compositions of Tables 1 and 2, Ag and Pd PIED has been performed successfully on TiO_2-sensitised quartz glass slides. The resultant layers, Fig. 4, are coherent, conductive and display a shiny, mirrored metallic finish. Deposits do not delaminate with metal-to-substrate adherence being demonstrated via British Standard metal adhesion test BS EN ISO 2819:1995. Also known as the 'scotch tape test', this involves an adhesive containing tape (scotch tape) being made to stick to the metal layer surface and then pulled out by applying a force. The metal layer is said to be adherent to the underlying substrate if it does not fail/delaminate under the said operation. Deposition only occurs on areas both sensitised with TiO_2 and irradiated with ultra-band gap light. Visual inspection and SEM analysis shows that, even after 2 h immersion in Ag and Pd electroless plating solutions, no deposition occurs on m-TiO_2-sensitised surfaces in the dark.

Longer deposition times result in thicker deposits, suggesting that extent of metal deposition can be controlled by deposition time. Interestingly, Ag samples prepared using an initial illumination time of 1800 s followed by 1800 s deposition in the dark have a similar visual finish to Ag samples prepared by 3600 s deposition with illumination throughout. This is consistent with the suggested mechanism of Fig. 2, wherein PIED occurs in two stages with photoinitiated nucleation being followed by autocatalytic metal deposition. In this context, the plating solution reductant (tartrate for Ag, hydrazine for Pd) participates in both stages, acting as a hole scavenger and then reductant during the first (Fig. 2(i)) and second (Fig. 2(ii)) stages respectively.

To further investigate the role of irradiation/nucleation time in PIED, m-TiO_2-coated quartz slides were illuminated in Ag electroless plating solution for periods of 30, 60, 120, 180, 240 and 300 s,

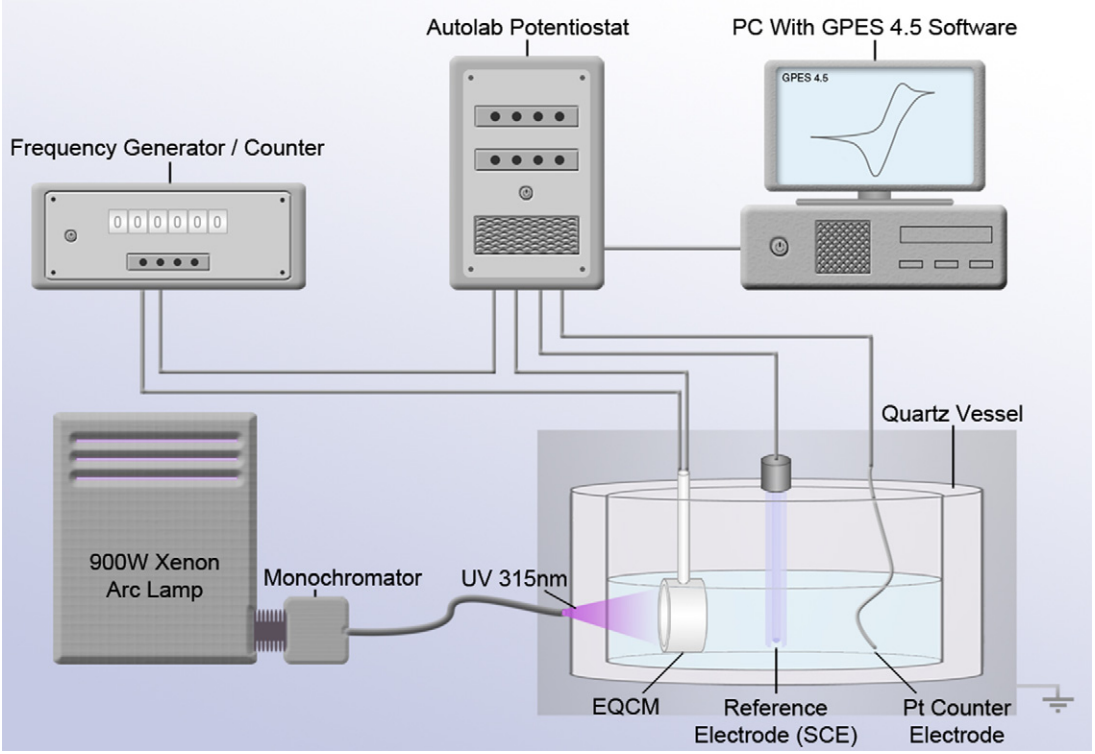

Fig. 3. Schematic of apparatus used for photoelectrochemical studies of PIED using the electrochemical quartz crystal microbalance (EQCM).

after which they remained immersed in solution in the dark for periods of 300, 600 and 900 s. As above, no deposition occurred on samples that had not undergone illumination. In contrast however, any period of illumination >30 s initiated a PIED process that produced coherent layers after a sufficient period of dark growth. Table 3 summarizes simple conductivity measurements of the resultant Ag layers where conductivity is indicated when zero resistance is measured between two conductance probes placed 25 mm apart on the sample surface. Conducting layers were produced when the combined light and dark plating time exceeded ~600 s.

As discussed above, the irradiation period promotes the formation of Ag nuclei on the TiO_2 surface. SEM images indicate that longer irradiation times and, by implication larger surface concentrations of metal nuclei, lead to metal deposits with a finer grain size and more reflective appearance, Fig. 5(a), whilst shorter illumination times and so fewer nuclei sites result in a coarser, more granular deposit structure, Fig. 5(b). Thus, longer irradiation/nucleation times are needed for higher reflectivity deposits.

PIED has also been used to deposit Ag, Fig. 6, and Pd onto nanoparticulate TiO_2-sensitised PVDF membranes. In both instances, deposited layers are conducting and metallic in appearance. Deposition can be applied to a single side of the membrane by floating it on the electroless plating solution surface, or on both sides by full immersion. No through membrane deposition or conductivity is observed.

Table 3
Summary of conductivity of PIED Ag layers on m-TiO_2-coated quartz.

Irradiation time	30s	60s	120s	180s	240s	300s
Dark 0 s	×	×	×	×	×	×
Dark 300 s	×	×	×	×	√	√
Dark 600 s	×	×	√	√	√	√
Dark 900 s	√	√	√	√	√	√

× = non-conducting and √ = conducting.

3.3. EQCM studies of PIED – silver

Cyclic voltammetry studies of ferricyannide (not shown) indicate that, once coated with m-TiO_2, approximately 64% of the Au piezoelectrode surface remains accessible to solution through the titania layer. Within the context of EQCM-based studies of PIED, Fig. 3, this Au surface accessibility may allow for Ag/Pd metal to be deposited by conventional electroless means onto the underlying Au piezoelectrode during a PIED experiment. Whilst the two effects would then need deconvoluting, the use of such piezoelectrode/TiO_2 composites allows for comparison of the electrochemical properties of uncoated crystals with those of illuminated and unilluminated m-TiO_2-coated crystals and thus the elucidation of key mechanistic information.

Using the set-up of Fig. 3, measurements at pH 11.5 show that the mixed potential (E_{mp}) of the Ag/tartrate system is +0.12 V whilst the flat band potential (E_{fb}, measured in-house from the photocurrent onset potential) of m-TiO_2 is −0.65 V. Due to this difference between E_{fb} and E_{mp}, significant band bending and space

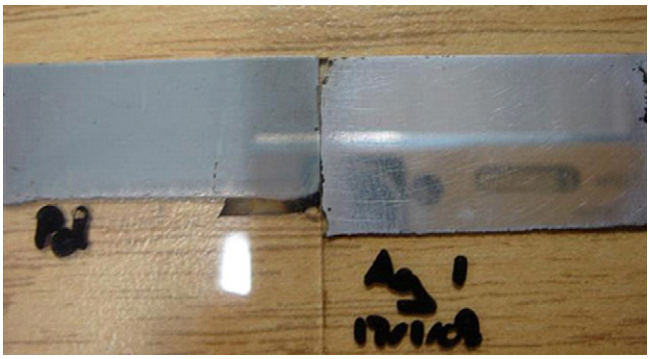

Fig. 4. Pd (left) and Ag (right) deposited by PIED onto the m-TiO_2-sensitised area of quartz slides. Samples irradiated with 315 nm light for 3600 s.

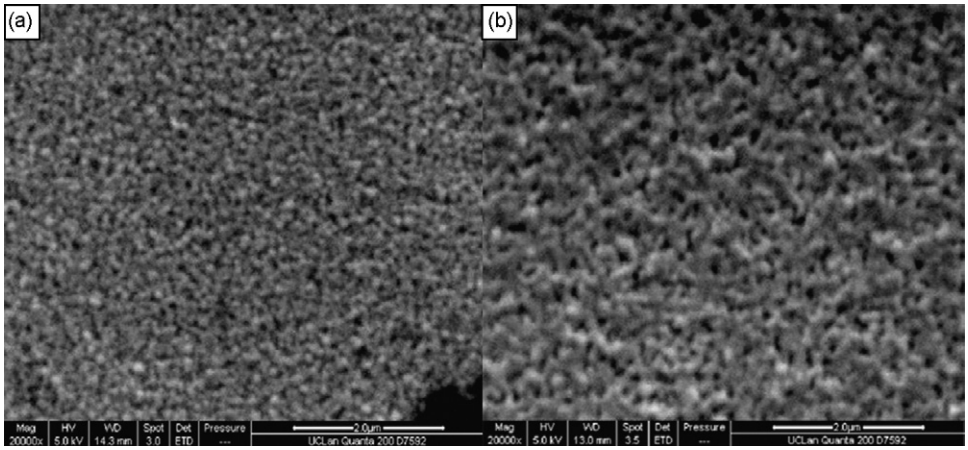

Fig. 5. SEM images of PIED-generated Ag deposit on m-TiO_2-coated quartz slides: (a) after 600 s continuous irradiation and (b) after 300 s irradiation followed by 300 s growth in the dark.

charge/depletion layer formation would be expected at the semiconductor–electrolyte interface at equilibrium in the dark [21]. At the resultant +0.77 V from flatband, the space charge layer thickness in the TiO_2 will be in the range 8–20 nm [22], compared to a primary constituent particle diameter of 15 nm [18], suggesting that majority carrier depletion occurs throughout the m-TiO_2 structure.

With these observations in mind, Fig. 7 shows the results of chronopotentiometry conducted during Ag PIED onto (a) a bare Au piezoelectrode in the dark, (b) an m-TiO_2-coated Au piezoelectrode in dark and (c) an m-TiO_2-coated Au piezoelectrode illuminated with 315 nm light. Both dark experiments, where $t = 0$ corresponds to the immersion of the piezoelectrode into the electroless plating solution, show similar results with a stable potential of +0.12 V as a function of immersion time, indicating that the presence of TiO_2 does not significantly affect E_{mp} in the dark. On irradiation, a negative shift of 75–100 mV from +0.12 V is seen, Fig. 7(c) where $t = 0$ corresponds to illumination onset. This may be understood through the action of the reducing agent, tartrate, as an effective TiO_2 hole scavenger, leading to an accumulation of photogenerated electrons within the semiconductor. This causes a negative shift in $(E_{mp} - E_{fb})$ and an unbending of the bands. We expect that this, in turn, will facilitate the transfer of photogenerated electrons to Ag (I) in solution and hence enhance the rate of metal nuclei formation (Fig. 2(i)). We shall return to this point below.

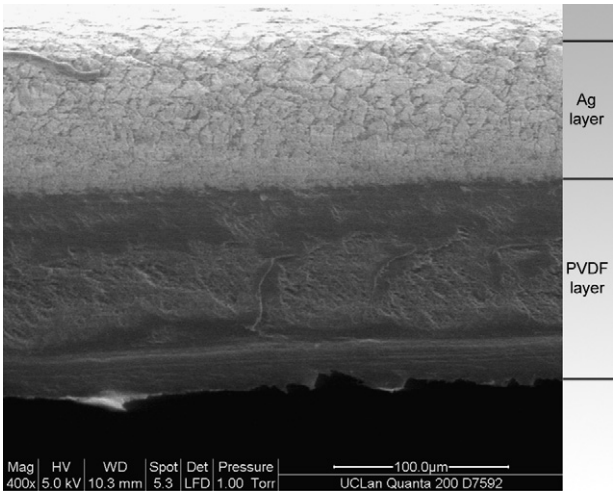

Fig. 6. Cross-sectional SEM image of PIED-generated Ag layer on PVDF membrane. Sample prepared by irradiating nanoparticulate TiO_2-sensitised PVDF membrane with 315 nm light for 1800 s.

Figs. 8 and 9 show simultaneously recorded gravimetric results for the samples of Fig. 7. Specifically, they show Δf and $d\,\Delta f/dt$ as functions of time, the latter being directly proportional to the metal deposition rate (see Section 2.7). All three traces in Fig. 8 display a frequency drop corresponding to a mass increase as metal deposition occurs.

As discussed above, no Ag growth occurs at the TiO_2/solution interface in the dark. Again as discussed above, Fig. 8(b) indicates that, for m-TiO_2-coated piezoelectrodes in the dark, conventional electroless deposition does indeed occur on the Au that remains accessible to the external solution through the TiO_2 layer. However, from Fig. 9(a) and (b), the rate of deposition at $t < 500$ s at the bare Au surface is ~50% greater than that seen at m-TiO_2-coated piezoelectrodes in the dark, suggesting that the TiO_2 is partially suppressing the rate of electroless deposition of Ag at the Au surface of the coated electrode by restricting access of the Ag(I) ion to that surface.

Fig. 9(a) and (c) shows that deposition onto the illuminated m-TiO_2 surface and bare Au have similar growth modes. The dark m-TiO_2 trace, Fig. 9(b), has a feature at ~580–800 s indicating a sharp increase in deposition rate followed by a sharp decrease followed eventually by a steady rate of deposition at $t > 1000$ s. The sharp increase at $t = 580$ s correlates with the point where growth *through* the TiO_2 layer is complete and Ag growth channels coalesce across the electrode surface. The decrease in rate at $t = 780$ s corresponds to the end of this period of lateral growth after which the layer grows perpendicular to the electrode surface and out into solution.

The feature observed at 580 s in Fig. 9(b) is predictably absent from Fig. 9(a) but is also missing from Fig. 9(c). We attribute this to the fact that, as mentioned, two simultaneous processes are occurring in the latter sample: (a) growth of a deposit by conventional electroless means from the Au electrode/m-TiO_2 interface through the m-TiO_2 layer, as per Fig. 9(b) and (b) Ag deposition at the outermost surface of the m-TiO_2 layer through PIED, as indicated by Fig. 7(c). Comparison of Fig. 9(c) with (a) leads us to conclude that the latter dominates in Fig. 9(c) as a result of (i) a photoinduced increase in electron concentration within the TiO_2 matrix and (ii) the unbending of the bands on illumination (vide supra), both of which result in an increase in electron access to the semiconductor–electrolyte interface so increasing the electrochemical activity of the m-TiO_2/piezoelectrode composite.

Eventually, at $t > 2000$ s all three systems grow in the same manner – specifically the metal layer grows into free solution by autocatalytic deposition in a direction perpendicular to the substrate surfaces. This similarity of behaviour is confirmed by the similarity of measured growth rates at $t = 6000$ s. At these long

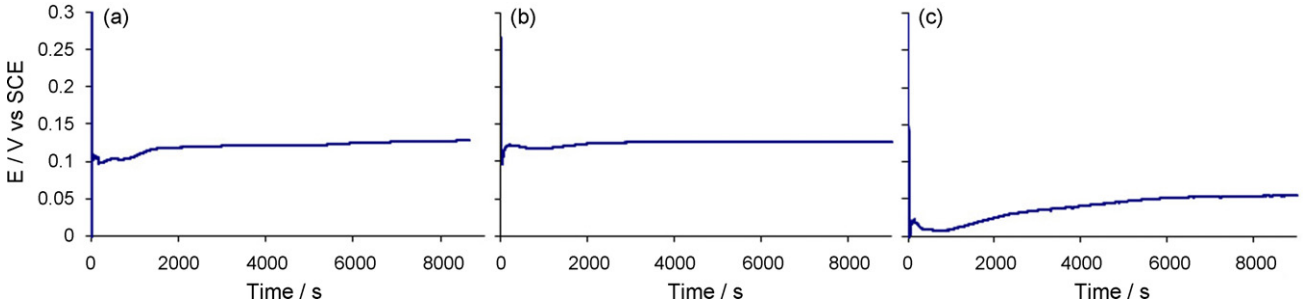

Fig. 7. Chronopotentiometric measurements for Ag PIED on (a) bare gold in the dark, (b) m-TiO_2-coated gold in the dark and (c) m-TiO_2-coated gold under ultra-band gap illumination.

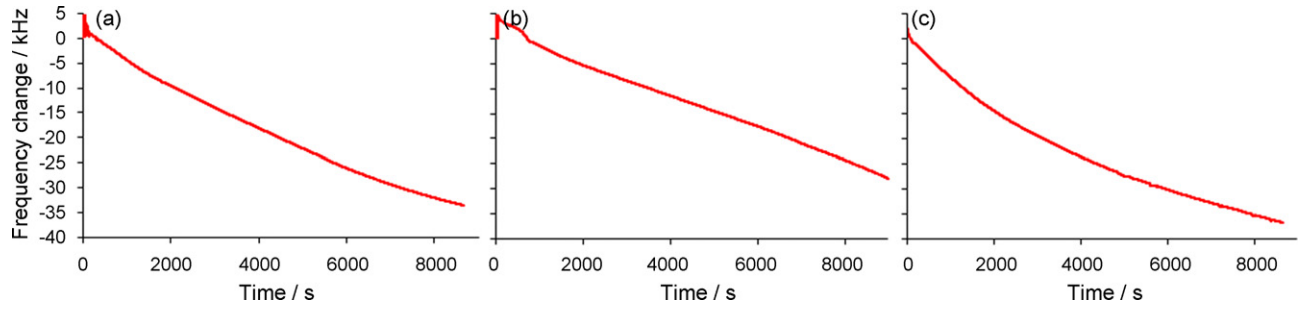

Fig. 8. QCM measurements showing change of frequency (mass) as a function of time for PIED of Ag/tartrate on (a) bare gold in the dark, (b) m-TiO_2-coated gold in dark and (c) m-TiO_2-coated gold in light.

deposition times, the metal is depositing as a coherent layer over the m-TiO_2 surface – consequently, Eq. (2) holds and deposition rate can be expressed in terms rate of change of layer thickness with time. Accordingly, on bare gold the growth rate is 1.01 nm min^{-1}, on m-TiO_2 in the dark the rate is 0.9 nm min^{-1} and on illuminated m-TiO_2 the rate is 0.6 nm min^{-1}. This rate is lower than that seen in the dark, possibly due to local depletion of the tartrate concentration at the metal growth front through photocatalytically driven oxidation processes. This growth rate equates to 0.88×10^{-6} g cm^{-2} min^{-1} which, given the differences in solution composition involved, compares well with that of 1.3×10^{-6} g cm^{-2} min^{-1} recorded by Kubota and Koura during the electroless deposition of Ag on a platinum electrode pre-sensitised with $SnCl_2$ [23].

3.4. EQCM studies of PIED – palladium

Gravimetry and chronopotentiometry were also used to monitor PIED of Pd, Figs. 10 and 11. The chronopotentiometric traces of Fig. 10 show that, at the initiation of deposition, E_{mp} values of −0.699 and −0.703 V are obtained for the bare and m-TiO_2-coated Au piezoelectrodes respectively in the dark. These are significantly negative of the analogous values recorded for the Ag/tartrate system of +0.12 V and are close to the measured E_{fb} of m-TiO_2 of −0.65 V. A measure of the thermodynamic driving force for metal deposition can be obtained by subtraction of the metal E^0 value from E_{mp}. This gives a driving force/overpotential of −1.3 V for Pd and −0.45 V for Ag, a difference reflected in the rates of deposition determined from Figs. 9 and 11.

From Tables 1 and 2, it can be seen that the concentration of Pd is twice that of Ag in their respective plating solutions. However, comparison of Figs. 9 and 11 indicates that peak deposition rates obtained from the Pd/hydrazine system at m-TiO_2-coated piezoelectrodes are at least 4.5× and up to 16× greater than those for the Ag/tartrate system. Specifically, peak rates for the Ag system are 9.9 Hz s^{-1} (from Fig. 9(b)) and 6.7 Hz s^{-1} (Fig. 9(c)) in the dark and light respectively, whilst peak rates for the Pd system are 49 Hz s^{-1} (Fig. 11(b)) and 56.8 Hz s^{-1} (Fig. 11(c)) in the dark and light respectively. Steady state rates at $t > 6000$ s (where Eq. (2) holds, vide supra) show similar trends where, from above, rates for Ag deposition are 3.56 Hz s^{-1} or 0.9 nm min^{-1} on m-TiO_2 in the dark and 2.4 Hz s^{-1} or 0.6 nm min^{-1} and under illumination. Analogous rates for the Pd system are 37.4 Hz s^{-1} or 8.7 nm min^{-1} in the dark and 40.9 Hz s^{-1} or 9.5 nm min^{-1} under illumination. The enhancement in Pd deposition rate with respect to Ag is at least in part derived from the difference in E_{mp} values observed, these in turn being determined by the reducing power of the reductant

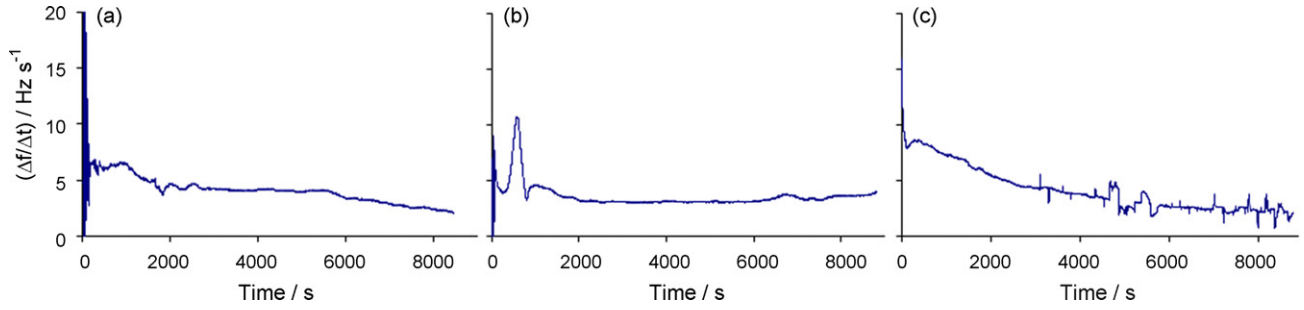

Fig. 9. QCM measurements showing the rate of change of frequency (rate of change of crystal mass) as a function of time for PIED of Ag/tartrate on (a) bare gold in the dark, (b) m-TiO_2-coated gold in dark and (c) m-TiO_2-coated gold in light.

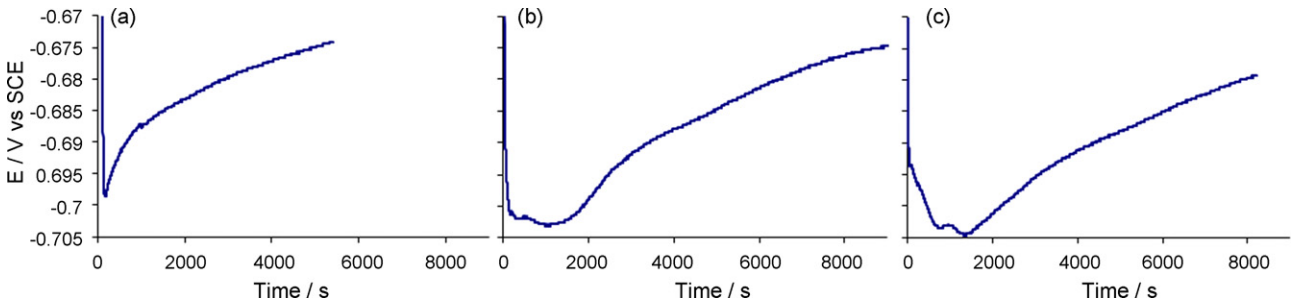

Fig. 10. Chronopotentiometric measurements for Pd PIED on (a) bare gold in the dark, (b) m-TiO_2-coated gold in the dark and (c) m-TiO_2-coated gold under ultra-band gap illumination.

employed. That a difference in the steady state deposition rate can be seen on variation of thermodynamic driving force for metal ion reduction indicates that, at the very least, Ag deposition in the Ag/tartrate system is under electrochemical control.

Illumination of the m-TiO_2-coated piezoelectrode with 315 nm light generates a small, 5 mV potential shift to −0.704 V, Fig. 10(c), from which the system then gradually recovers. Again, this is in contrast to the Ag/tartrate system, where a significantly larger change in E_{mp} of 75–100 mV occurs upon illumination (Fig. 7(a)). Given the proximity of E_{mp} for the Pd/hydrazine system to the flat band potential of −0.65 V of our m-TiO_2, we would expect little to no band bending in the dark, that which does exist leading to the formation of a very shallow accumulation layer. Further, given the small change in E_{mp} upon illumination, we expect little difference in the light with virtually no photogenerated band bending superimposed on the putative shallow accumulation layer formed in the dark. This accumulation layer might be expected to lead, in the dark or light, to greater ease of access of majority charge carriers to the semiconductor–electrolyte interface in the TiO_2/Pd/hydrazine system compared to the TiO_2/Ag/tartrate system, so enhancing the rate of nucleation (Fig. 2(i)) and, ultimately, deposition (Fig. 2(ii)). However, this will be offset by the shallowness of the band bending providing little driving force for photogenerated charge separation in the TiO_2/Pd/hydrazine system, resultant recombination suppressing the free electron concentration and the so the nucleation rate of Fig. 2(i). This lower nucleation rate notwithstanding, the more negative value of E_{mp} in the Pd/hydrazine system compared with the Ag/tartrate system will, in the case of the former, produce higher rates of autocatalytic deposition (Fig. 2(ii)) at those nucleation centres that do form. This accelerated rate of deposition at fewer nucleation centres in the Pd system would be expected to give rise to a more granular, less reflective deposit than in the Ag system with its faster rate of (charge separation assisted) nucleation and slower (tartrate driven) autocatalytic growth. Comparison of the photographs of PIED derived Ag and Pd layers of Fig. 4 shows that this is indeed what is seen, an observation that is further supported by comparison of the SEM images of Fig. 12.

In light of the preceding relating to the Pd system and the earlier discussion of the Ag system, the form of the QCM traces of Fig. 11 may be understood as follows. For the uncoated piezoelectrode in the dark, Fig. 11(a), there is first an induction period of ~40 s during which conventional Pd-on-Au nucleation is initiated, a phenomenon typical of most electroless deposition processes. This is then followed by a period of deposition rate acceleration, reaching a peak at ~200 s, as nucleation sites are formed and nucleate growth begins. Finally, at $t > 200$ s, the rate decreases as nuclei coalesce through lateral growth and precursor metal ion depletion occurs into solution. Once the surface is covered, deposition reaches a stable rate determined by the balance between E_{mp} controlled electrochemical kinetics and mass transfer.

Analogous processes occur at the m-TiO_2-coated piezoelectrodes. A period of Pd-on-Au nucleation at the TiO_2/Au interface at $t < 400$ s (most clearly seen in Fig. 11(c)) is followed by a period of steady Pd layer growth/deposition through the m-TiO_2 layer. At $t < 1000$ s, the $d\,\Delta f/dt$ vs. time plots of Fig. 11(b) and (c) clearly show a suppression in rate of deposition at m-TiO_2-coated compared to bare piezoelectrodes, Fig. 11(a). As in the Ag results of Fig. 9, this is due to the inhibition of solution phase mass transport of Pd(II) to the Au surface in the presence of the m-TiO_2 layer.

At $t > 1000$ s, in both light and dark, the m-TiO_2-coated samples show an acceleration in deposition rate as the deposition fronts emerge from the mesoporous structure of the TiO_2 and growth channels spread laterally across the semiconductor, coalescing to form a coherent metal surface. Once coalescence is complete, characterized by a peak in the deposition rate, the deposition rate relaxes to a stable rate as per the uncoated piezoelectrodes. As discussed above with relation these steady state rates for the Pd system can be as much as 8–16× greater than the equivalent rates for the Ag system, due in no small part to the greater reductive power of hydrazine compared to tartrate.

As per the Ag system, two simultaneous processes are occurring in the Pd deposition experiments of Fig. 11: (a) deposit growth by conventional electroless means from the Au electrode/m-TiO_2 interface and (b) metal deposition at the m-TiO_2/solution interface

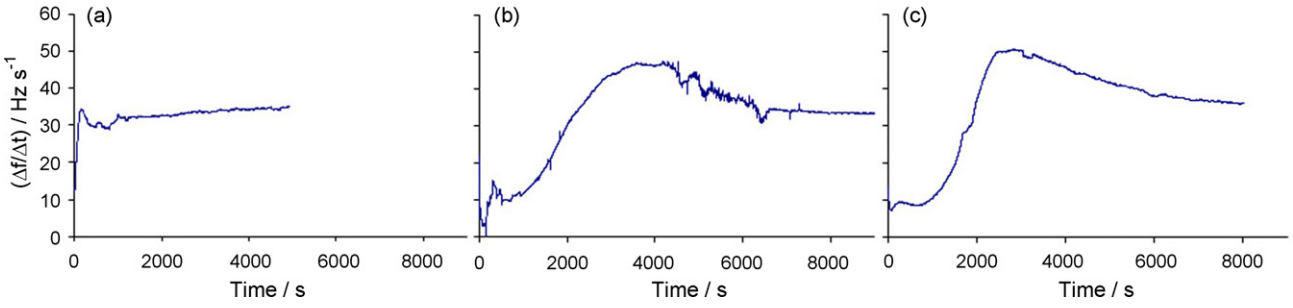

Fig. 11. QCM measurements showing the rate of change of frequency (mass) as a function of time for PIED of Pd on (a) bare gold in the dark, (b) m-TiO_2-coated gold in dark and (c) m-TiO_2-coated gold in light.

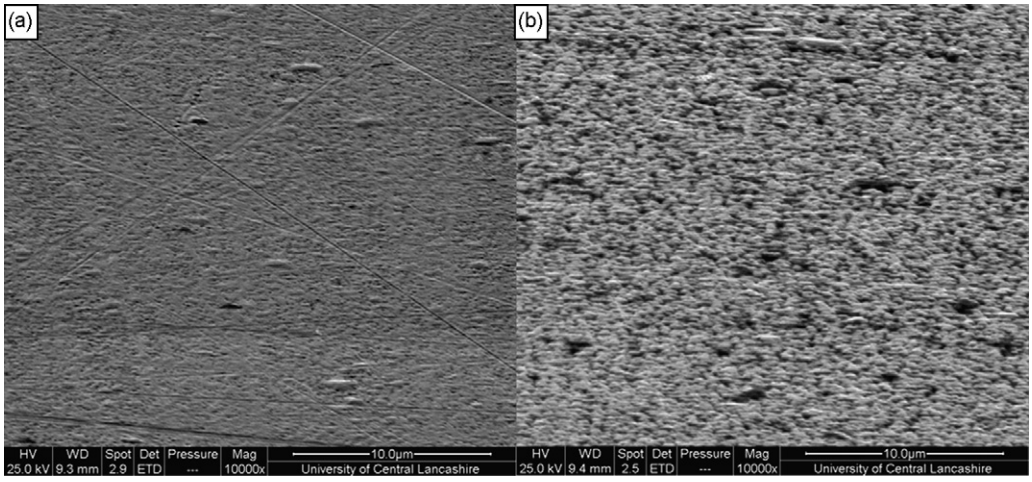

Fig. 12. SEM images of (a) an Ag deposit and (b) a more granular Pd deposit, generated by PIED on m-TiO_2-coated quartz slides. Samples irradiated with 315 nm light for 3600 s. Plating solution compositions given in Tables 1 and 2.

through PIED. Comparison of Fig. 11(c) and (b) indicates that, in contrast to the Ag/tartrate system, the former process is dominating in Fig. 11(c).

This is not to discount a contribution by PIED to the result of Fig. 11(c). In the dark, the peak deposition rate of 49 Hz s^{-1} on coated electrodes is reached at ~4000 s whilst under illumination the peak rate of 56.8 Hz s^{-1} is reached after ~2800 s. This is consistent with a PIED enhancement in the nucleation/deposition rate running in parallel with conventional electroless deposition occurring at the Au/TiO_2 interface. As indicated by Figs. 4 and 12, PIED is fully effective in the generation of Pd layers on wholly insulating substrates where it will be the only initiating process.

4. Conclusions

We report a novel one-step photocatalytically initiated electroless deposition (PIED) process that allows for the photogeneration of coherent and conducting metal layers on semiconductor-sensitised insulator surfaces. Deposition occurs only onto those areas of the substrate both sensitised with TiO_2 and irradiated with ultra-band gap light, so suggesting the future development of PIED driven photo-microlithography. PIED obviates the need for Sn–Pd activation catalysts so eliminating contamination from prior nucleation whilst the fewer steps and materials required provide a cheaper, environmentally cleaner and (through variation of incident light intensity) more controllable option than the traditional techniques of dielectric plating. Using PIED, Ag and Pd layers have been generated on m-TiO_2-coated quartz and PVDF substrates.

Through judicious choice of a hole scavenger that can also act as a reductant in an electroless deposition process, the PIED process allows for the metal nucleation and growth stages to be conducted simultaneously. The former process is driven by photocatalytically promoted metal ion reduction, whilst the latter proceeds autocatalytically on the resultant metal nuclei. SEM and EQCM studies indicate that the morphology and appearance of the resultant metal layer is strongly dependent upon the nucleation density arising during the primary photocatalytic stage of PIED. High nucleation density and a slow nuclei growth rate, such as obtained on m-TiO_2-sensitised surfaces in the Ag/tartrate electroless plating system, result in a smooth, reflective layer. A lower nucleation density combined with fast nuclei growth, as in the Pd/hydrazine system, results in a less reflective and often dull grey metal surface.

In the case of Ag deposition using a tartrate reductant, mixed potential (E_{mp}) measurements at m-TiO_2-coated Au piezoelectrodes indicate that E_{mp} shifts by up to −100 mV upon irradiation during PIED. This would be expected to lead to an unbending of bands within the semiconductor matrix, enhancing the availability of photogenerated electrons at the semiconductor surface with a consequent increase in metal nucleation rate. QCM measurements confirm that this is indeed the case with photoinitiated nucleation rates being larger than those seen on bare metal substrates.

In the case of Pd deposition using a hydrazine reductant, E_{mp} measurements at m-TiO_2-coated Au piezoelectrodes indicate that the TiO_2 layer is at near flat band in both the dark and when illuminated with ultra-band gap light. The resultant lack of driving force for charge carrier separation leads to a higher recombination rate for this system compared to that of Ag with a consequent lower rate of photoinitiated nucleation, as determined by microgravimetry. This lower nucleation density, combined with the rapidity of growth afforded by hydrazine reductant (indicated by QCM experiments), results in the Pd deposit having a coarser morphology than that of the Ag deposit.

In light of the above, we can conclude that high reflectivity deposits with small grain sizes are favoured by (i) high nucleation rates and consequent high nuclei densities (achieved through use of good hole scavengers and long illumination times) and (ii) slow nuclei growth rates (achieved through use of hole scavengers that are poor reductants in conventional electroless deposition processes). The thickness of the final deposit can be controlled through the deposition (as opposed to illumination) time

Acknowledgements

The authors wish to thank the organizers of SP-3 for the invitation to submit this paper. The authors also wish to thank the Royal Society of Chemistry UK for studentships for MAB and SG, and Sellafield Ltd, the Nuclear Decommissioning Authority (NDA) and The Lloyds Register Educational Trust for financial support. The Lloyds Register Educational Trust is an independent charity working to achieve advances in transportation, science, engineering and technology education, training and research worldwide for the benefit of all.

Appendix A. Supplementary data

Supplementary data associated with this article can be found, in the online version, at doi:10.1016/j.jphotochem.2010.07.029.

S1, Raman spectroscopic characterization of m-TiO_2 films; S2, UV–vis spectroscopic characterization of m-TiO_2 films; S3, AFM characterization of m-TiO_2 films.

References

[1] D. Kunces, Chemical deposition of metallic films from aqueous solution, in: G.O. Mallory, J.B. Hajdu (Eds.), Electroless Plating – Fundamentals and Applications, American Electroplater & Surface Finishers Society, Orlando, FL, 1990, pp. 511–517.
[2] M. Paunovic, M. Schlesinger, Electroless Deposition, Fundamentals of Electrochemical Deposition, 2nd ed., 2006, pp. 139–167.
[3] J.J. Kuzmik, Plating on plastics, in: G.O. Mallory, J.B. Hajdu (Eds.), Electroless Plating – Fundamentals and Applications, American Electroplater & Surface Finishers Society, Orlando, FL, 1990, pp. 377–399.
[4] C.R. Shipley, US Patent 3,011,920, 1961.
[5] A. Mills, S. Le Hunte, Journal of Photochemistry and Photobiology A: Chemistry 108 (1997) 1.
[6] H. Chun, J. Kim, S.M. Yoon, C. Kim, Korean Journal of Chemical Engineering 18 (2001) 908.
[7] J.W.M. Jacobs, The Journal of Physical Chemistry 90 (1986) 6507.
[8] V. Vamathevan, R. Amal, D. Beydoun, G. Low, S. McEvoy, Journal of Photochemistry and Photobiology A: Chemistry 148 (2002) 233.
[9] M.I. Litter, Applied Catalysis B: Environmental 23 (1999) 89.
[10] S. Sato, J.M. White, Chemical Physics Letters 72 (1980) 83.
[11] E. Stathatos, P. Lianos, P. Falaras, A. Siokou, Langmuir 16 (2000) 2398.
[12] L.Q. Wu, N. Xu, J. Shi, Industrial & Engineering Chemistry Research 39 (2000) 342.
[13] L.Q. Wu, N. Xu, J. Shi, AIChE Journal 46 (2000) 1075.
[14] X. Li, Y. Fan, W. Jin, Y. Huang, N. Xu, J. Shi, Desalination 192 (2006) 117.
[15] X. Li, Y. Fan, W. Jin, Y. Huang, N. Xu, Journal of Membrane Science 282 (2006) 1.
[16] Y.A. Yang, Y.B. Wei, B.H. Loo, J.N. Yao, Journal of Electroanalytical Chemistry 462 (1999) 259.
[17] K. Akamatsu, A. Kimura, H. Matsubara, S. Ikeda, H. Nawafune, Langmuir 21 (2005) 8099.
[18] J.C. Yu, J. Yu, W. Ho, J. Zhao, Journal of Photochemistry and Photobiology A: Chemistry 148 (2001) 331.
[19] S. Bruckenstein, M. Shay, Journal of Electroanalytical Chemistry 189 (1985) 131.
[20] Z.X. Shu, S. Bruckenstein, Journal of Electroanalytical Chemistry 317 (1991) 263.
[21] A.J. Bard, L.R. Faulkner, Photoelectrochemistry and Electrogenerated Chemiluminescence, Electrochemical Methods: Fundamentals and Applications, 2nd ed., 2001, pp. 746–752.
[22] R. Beranek, H. Tsuchiya, T. Sugishima, J.M. Macak, L. Taveira, S. Fujimoto, H. Kisch, P. Schmuki, Applied Physics Letters 87 (2005) 243114.
[23] A. Kubota, N. Koura, Journal of the Metal Finishing Society of Japan 37 (1986) 131.